Bifurcations and multiple traffic jams in a car-following model with reaction time delay

Gábor Orosz *, Bernd Krauskopf, and R. Eddie Wilson

Bristol Centre for Applied Nonlinear Mathematics,
Department of Engineering Mathematics, University of Bristol,
Queen's Building, Bristol BS8 1TR, United Kingdom

Abstract

We investigate an optimal velocity car-following model for n cars on a circular single-lane road, where reaction time delay of drivers is taken into account. The stability of the uniform-flow equilibrium is studied analytically, while bifurcating periodic solutions for different wave numbers are investigated with numerical continuation techniques. This reveals that the periodic solution with the smallest wave number may be stable, and all other periodic solutions are unstable.

As n is increased, periodic solutions develop stop- and go-fronts that correspond to rapid deceleration and acceleration between regions of uniformly flowing and stagnant traffic. In terms of the positions of all cars on the ring these fronts are associated with traffic jams. All traffic jams form a traffic pattern that evolves under time, due to slow motion of the fronts. The traffic pattern corresponding to the stable periodic motion of cars is the only stable one. However, we find that other periodic orbits may be unstable only so weakly that they give rise to transient traffic jams that may persist for long times. Eventually such traffic jams either merge with one another or disperse, until the stable traffic pattern is reached.

Key words: Traffic modelling, reaction time delay, periodic solutions, Floquet multipliers, front dynamics, traffic patterns
PACS: 05.45.-a, 45.70.Vn, 47.54.+r

* Corresponding author
Email addresses: g.orosz@bristol.ac.uk (Gábor Orosz), b.krauskopf@bristol.ac.uk (Bernd Krauskopf), re.wilson@bristol.ac.uk (R. Eddie Wilson).

1 Introduction

This article is concerned with the application of dynamical systems techniques to a well-known *car-following* model of highway traffic, called the *Optimal Velocity* model. Identical vehicles are modelled as discrete entities that move in continuous time and one-dimensional space along a circular single-lane road. The model that we consider here (see Section 2 for details) incorporates the reaction-time delay of drivers and was first posed by Davis [1]. It consists of a system of delay differential equations (DDEs) and is a variation of the reaction-time model introduced by Bando *et al.* [2], which in turn generalizes their original Optimal Velocity model [3]. This original work by Bando *et al.*, along with the work of Nagel and Schreckenberg [4] (on cellular automata models) and of Kerner and Konhäuser [5] (on partial differential equation models) has generated a surge of interest in the nonlinear behavior of highway traffic. For a comprehensive review, see Helbing [6]. Most studies have investigated dynamics by using a combination of numerical simulation and simple analytical arguments, such as linear stability analysis. Only recently [7,8] have formal dynamical systems techniques been used to classify different traffic behaviors.

The global dynamics of the OV model that we consider here were probed by numerical simulation in [1]. In contrast, in [7] we used the package DDE-BIFTOOL [9] to perform a two-parameter bifurcation analysis of the model. Due to the demands on CPU time and memory, the aim of [7] was proof-of-concept only, and the investigation was restricted to the unrealistic setting of $n = 3$ cars. Nevertheless, this methodology enabled us to calculate efficiently branches of periodic solutions (loosely corresponding to traffic jams) far from the *uniform flow equilibrium*, and to classify regions of parameter space where the equilibrium is stable yet coexists with other non-trivial stable solutions. In such bistable regions of parameter space, the choice of initial conditions selects which traffic behavior is selected as time $t \to \infty$.

In this paper the goal is to extend the results to larger n, and in particular to draw out the trends which may emerge as n is increased towards numbers that are more representative of real traffic situations. The present limit of our computation is $n = 17$ cars: this is still restricted but nevertheless begins to display some of the interesting wave interaction phenomena that one may find (by numerical simulation) for large n.

Of particular interest is the interplay between periodic solutions and traffic patterns. As observed by many other authors, for appropriate parameters and initial data, traffic organizes into regions of free flowing traffic divided by traffic jams which propagate at about the same speed to each other in the opposite direction to the traffic flow. The question is how such traffic patterns evolve.

The traffic jams correspond to regions in which the gradient of the trajectories (*i.e.*, vehicles' velocities) is small; see already Figs. 11 and 12 in Section 9. The key point to note is that, although different traffic jams have similar speeds, and so they may co-exist over intermediately long time scales, as $t \to \infty$ they have a tendency to merge (Fig. 11(a)). Further, over sufficiently long time scales, traffic jams may also disperse (Fig. 12(a)). Consequently, for generic choices of initial data, only a single traffic jam persists as $t \to \infty$.

To understand traffic patterns one needs to consider the dynamics of a single vehicle as it drives repeatedly around the circuit. The velocity plateaus at a high value, meets a 'stop front' in which the vehicle decelerates into a traffic jam, plateaus at a low value, and then passes through a 'go front' as it returns to free flow conditions. Consequently a traffic jam is sometimes known as 'stop-and-go wave', although we should emphasize that each traffic jam is strictly speaking a pair of waves with similar speeds, separated by a low-velocity plateau. Since (apart from at merging) the stop-and-go waves propagate at about the same speed, the motion of the vehicle is approximately periodic in time because it encounters the same traffic pattern for each circuit, albeit shifted according to the wave speed. This observation motivates the detailed study of perfectly periodic orbits which we perform first at the linear level (Section 4) and then at the fully nonlinear level in terms of two-parameter bifurcation diagrams (Section 5).

In particular, we find regions of parameter space where a stable periodic solution with $k = 1$ traffic jams coexists with unstable periodic solutions corresponding to $k > 1$ perfectly evenly spaced traffic jams. For large n/k, we show that the 'stop fronts' and 'go fronts' have a limiting structure. This result indicates that we have recovered fronts which are close to travelling wave solutions in the case of open boundaries, and which only feel the other waves weakly since the number of vehicles ($\sim n/k$) between structures is large. By computing Floquet multipliers of periodic orbits we show that periodic solutions for $k > 1$ may be only weakly unstable; the unstable eigendirections show that the mechanism of destabilization is via front dynamics. Both the Floquet multiplier and mode shape calculations that we perform can only be achieved with numerical continuation software such as DDE-BIFTOOL [10,11].

We find that the largest Floquet multiplier μ has a scaling of $|\mu| - 1 \sim \exp(-\text{const. } n/k)$. This indicates that our periodic solutions correspond to travelling wave solutions when the boundaries are open, but on the loop interact weakly via their exponential decaying tails (in a similar manner to metastable front dynamics for the Allen-Cahn equation; see [12,13]). We show that eigendirections correspond to relative front motion: either one stop-and-go pair catching up another stop-and-go pair (merging of traffic jams), or the stop-and-go fronts of a single jam colliding so as to disperse it.

The paper is organized as follows. In Section 2 we give details of the model. Section 3 gives some background on the stability theory for DDEs with a single fixed delay, while Section 4 contains the linear stability analysis of the uniform flow solution. In Section 5 we present the two-parameter bifurcation diagrams for $n = 3, 5, 9$ cars. The associated branches of periodic solutions (also for $n = 17$) are discussed in Section 6. How fronts develop in periodic solutions is shown in Section 7. The Floquet multiplier and eigendirection calculations can be found in Section 8. Merging and dispersing transient traffic jams are explained in Section 9. We conclude in Section 10.

2 Model details

The model described here is based on those of [1–3] and was set up and rescaled in [7]. We consider a system of n cars on a unidirectional single-lane ring road of length L. The velocity of the i-th vehicle is denoted v_i and its distance to the preceding $i+1$-th vehicle, known as the *headway*, is denoted by h_i. We thus have the kinematic conditions

$$\dot{h}_i(t) = v_{i+1}(t) - v_i(t), \quad i = 1, \ldots, n, \tag{1}$$

and the model is closed by prescribing cars' accelerations in the non-dimensionalized form

$$\dot{v}_i(t) = \alpha \left[\mathrm{V}\left(h_i(t-1)\right) - v_i(t) \right], \quad i = 1, \ldots, n. \tag{2}$$

Throughout we identify the $n+1$-th car with the first car, so that $\dot{h}_n(t) = v_1(t) - v_n(t)$, and the length of the ring is included in the model via the condition

$$\sum_{i=1}^{n} h_i = L\,. \tag{3}$$

In particular, we define $h_n = L - \sum_{i=1}^{n-1} h_i$, which reduces the number of independent equations of Eqs. (1)–(2) to $2n-1$.

Equation (2) expresses that each driver approaches an *optimal velocity* (OV), given by $\mathrm{V}(h) \geq 0$, with a characteristic *relaxation time* of $1/\alpha > 0$. Further, drivers react to their headway via a *reaction time delay* which here is rescaled to one. The parameter $\alpha > 0$ is known as the *sensitivity*. Since we want to compare results for different numbers of cars n, we consider the *average headway* $h^* = L/n$ as a bifurcation parameter. Increasing h^* increases the length of the ring, L, which involves scaling all headways h_i accordingly.

To complete the model we specify the *OV function* $V(h)$. The remainder of

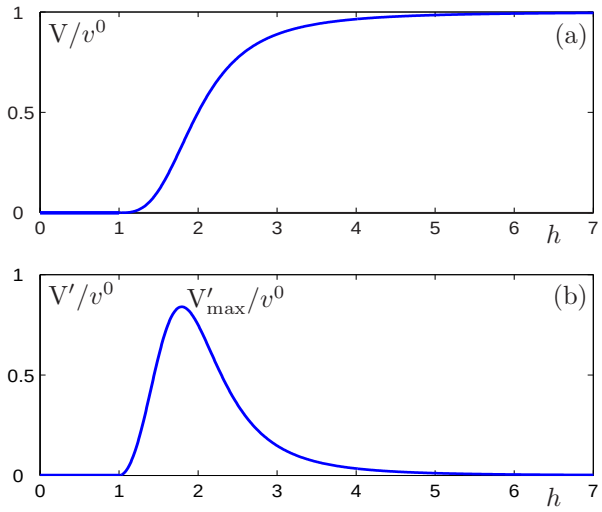

Fig. 1. Optimal Velocity function (4) (a), and its derivative (b).

this paper uses the rescaled form

$$\mathrm{V}(h) = \begin{cases} 0 & \text{if} \quad 0 \le h \le 1\,, \\ v^0 \dfrac{(h-1)^3}{1+(h-1)^3} & \text{if} \quad h > 1\,, \end{cases} \tag{4}$$

first introduced in [7], which is shown together with its derivative in Fig. 1, and which has the following properties:

1. $\mathrm{V}(h)$ is continuously differentiable, nonnegative, and monotone increasing. So in particular, cars tend to travel faster as their headway increases. Note that the smoothness is required for the application of continuation techniques later in this paper.

2. $\mathrm{V}(h) \to v^0$ as $h \to \infty$, where v^0 is known as the *target speed*, which corresponds to the (high) free-flow speed of drivers when traffic is sparse.

3. $\mathrm{V}(h) \equiv 0$ for $h \in [0, 1]$, so that one is the rescaled *jam headway*. If a vehicle's headway becomes less than one it should attempt to come to a stop, although in fact in model (2) its speed may only decay exponentially to zero.

Note that functions with similar shapes and properties to (4) were used in [2,3].

3 Delay differential equations with a single time delay

Equations (1)–(2) constitute a system of $2n-1$ independent delay differential equations (DDEs) with a single fixed delay that is scaled to 1. We now recall some basic facts of the stability theory for DDEs as needed in later sections; see [14–17] for more details. In general form, such a system can be written as

$$\frac{dx(t)}{dt} = f(x(t), x(t-1), \eta)\,, \tag{5}$$

where $x \in \mathbb{R}^m$ is the physical space, and $f\colon \mathbb{R}^m \times \mathbb{R}^m \times \mathbb{R}^l \to \mathbb{R}^m$ is differentiable, and $\eta \in \mathbb{R}^l$ is a (multi-dimensional) parameter. (In the case of Eqs. (1)–(2) $m = 2n-1$ and $l = 3$, which corresponds to the parameters h^*, α and v^0.) Due to the delay, initial data must be prescribed in the form of a continuous function on the interval $[-1, 0]$. Therefore, the phase space of (5) is the infinite-dimensional space $\mathcal{C}([-1,0], \mathbb{R}^m)$ of continuous functions over the delay interval with values in the physical space $\mathbb{R}^m$.

At an *equilibrium* we have $x^*(t) \equiv x^* \in \mathbb{R}^m$. The stability near $x^*(t)$ is given by the linearized system

$$\frac{dy(t)}{dt} = \mathrm{L}y(t) + \mathrm{R}y(t-1)\,, \tag{6}$$

where $y(t) = x(t) - x^*(t)$ and $\mathrm{L}, \mathrm{R} \in \mathbb{R}^{m\times m}$ are constant matrices (that depend on the parameter η). By inserting trial solutions in the form $y(t) = ce^{\lambda t}$ into (6) one obtains the characteristic equation

$$\det(\lambda \mathrm{I} - \mathrm{L} - \mathrm{R}e^{-\lambda}) = 0\,. \tag{7}$$

Equation (7) has infinitely many roots, the *characteristic exponents* $\lambda \in \mathbb{C}$, which have no accumulation point in $\mathbb{C}$. The equilibrium $x^*(t)$ is stable when all characteristic exponents are situated in the left half of the complex plane. If a real characteristic exponent crosses the imaginary axis then a fold (saddle-node) bifurcation occurs. (Note that we do not encounter this bifurcation in Eqs. (1)–(2)). If a pair of complex conjugate characteristic exponents crosses the imaginary axis then a Hopf bifurcation occurs. At the Hopf bifurcation a small-amplitude periodic solution bifurcates, which may be stable or unstable (of saddle type), depending on whether the Hopf bifurcation is supercritical or subcritical.

A periodic solution is of the form $x_\mathrm{p}(t) = x_\mathrm{p}(t+T)$, where $T \in \mathbb{R}$ is the period. To determine the stability of a periodic solution one considers the variational equation

$$\dot{z}(t) = \mathrm{L}_\mathrm{p}(t)z(t) + \mathrm{R}_\mathrm{p}(t)z(t-1)\,, \tag{8}$$

where $z(t) = x(t) - x_p(t)$ and the matrix functions $\mathrm{L_p}, \mathrm{R_p} \colon \mathbb{R} \to \mathbb{R}^{m\times m}$ are T-periodic. By integrating (8) over the period T one obtains the Floquet or monodromy operator whose eigenvalues are the *Floquet multipliers*. For the case of a fixed delay considered here the Floquet multipliers have the origin as their only accumulation point. Note that there is always the trivial Floquet multiplier $\mu = 1$, which corresponds to the time-translation symmetry along the periodic orbit. The periodic solution $x_\mathrm{p}(t)$ is stable when all Floquet multipliers (except the trivial one) are situated inside the unit circle in the complex plane. When Floquet multipliers cross the unit circle one encounters a bifurcation. In this paper we only find the case of a fold (saddle-node) bifurcation of periodic solutions, which occurs when a real Floquet multiplier crosses the unit circle at $+1$. Note that, in general, the Floquet multipliers cannot be written in closed form. They must be computed numerically, either by semi-discretization [18] or by full discretization [9].

Our principal tool is the numerical continuation package DDE-BIFTOOL [9,10] which is able to follow branches of equilibria and periodic solutions of DDE systems as parameters are changed. Stability information is computed along solution branches. Codimension-one bifurcation points where the stability of solutions changes are detected automatically. In particular, we may follow the branches of periodic solutions that are born at Hopf bifurcations and detect subsequent secondary bifurcations such as fold (saddle-node) bifurcations. Furthermore, the Floquet multipliers and the corresponding eigendirections are available from DDE-BIFTOOL. This allows us to identify characteristic time scales of repulsion when the solutions are unstable.

A periodic solution is represented in DDE-BIFTOOL by a number of mesh points, with a (small) number of so-called collocation points in between them. On each mesh interval the solution is represented by a polynomial, and the number of collocation points defines its degree. We used an accuracy of 50 mesh points and 3 collocation points for most calculations, but increased this to 60 mesh points and 5 collocation for the calculation of eigendirections in Section 8.

Overall, DDE-BIFTOOL performs similar functions for DDE systems as the well known package AUTO [19] performs for ODE systems. In general, the application of continuation packages such as AUTO and DDE-BIFTOOL is a much more efficient way of exploring parameter space than performing mass ensemble simulation of the initial value problem.

4 Linear stability analysis

The simplest solution of system (1)–(2), the so-called *uniform flow equilibrium*, is given by

$$h_i(t) \equiv h^* = L/n\,, \quad v_i(t) \equiv \mathrm{V}(h^*)\,, \tag{9}$$

for $i = 1, \ldots, n$. In other words, equidistant cars move with the same time-independent velocity. To investigate the stability of this equilibrium we consider the linearization of (2)

$$\dot{v}_i(t) = -\alpha v_i(t) + \alpha \mathrm{V}'(h^*) r_i(t-1)\,, \tag{10}$$

with the kinematic condition

$$\dot{r}_i(t) = v_{i+1}(t) - v_i(t)\,, \tag{11}$$

for $i = 1, \ldots, n$, where $r_i(t) = h_i(t) - h^*$. From this we obtain the characteristic equation in the form

$$\left(\lambda^2 + \alpha\lambda + \alpha \mathrm{V}'(h^*) e^{-\lambda}\right)^n - \left(\alpha \mathrm{V}'(h^*) e^{-\lambda}\right)^n = 0\,. \tag{12}$$

To find curves of Hopf bifurcations in parameter space we substitute $\lambda = \mathrm{i}\omega$, $\omega \in \mathbb{R}$, into (12). Separation of the real and imaginary parts gives

$$\begin{aligned} \mathrm{V}'(h^*) &= \frac{\omega}{2\cos(\omega - k\pi/n)\sin(k\pi/n)}\,, \\ \alpha &= -\omega \cot(\omega - k\pi/n)\,, \end{aligned} \tag{13}$$

for the set in parameter space where Hopf bifurcations occur. Here $k = 1, \ldots, n-1$ is known as the discrete spatial wave number because the spatial pattern of the bifurcating periodic solution is described by

$$\mathrm{Re}(c_i) = \cos\left(\frac{2\pi k}{n} i\right)\,, \quad \text{for } i = 1, \ldots, n. \tag{14}$$

Equations (13) describe curves in the $(\mathrm{V}'(h^*), \alpha)$-plane. Each curve belongs to a particular wave number k and is parameterized by the frequency $\omega \in (0, k\pi/n)$. However, we are only interested in the curves for $k \leq n/2$ because those for $k > n/2$ correspond to conjugated waves, *i.e.*, to the same spatial patterns. When n is even, the Hopf bifurcation curve for $k = n/2$ starts ($\omega = 0$) from the point $(1/2, 0)$ but all other Hopf bifurcation curves, for n even or odd and for any k, start from the origin. Further, all curves converge to the vertical asymptotes

$$\mathrm{V}'(h^*) = \frac{k\pi/n}{2\sin(k\pi/n)} \tag{15}$$

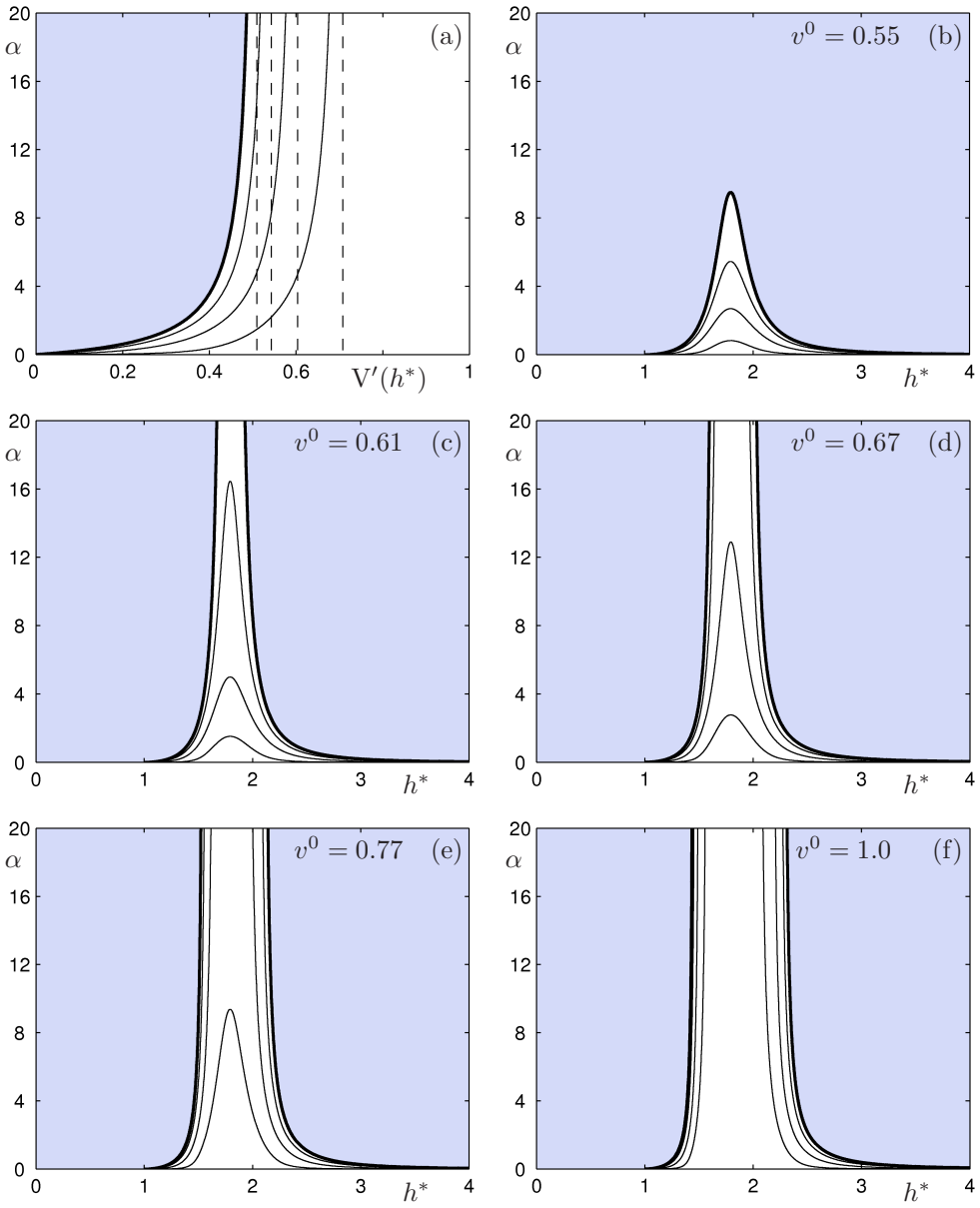

Fig. 2. Stability diagrams for $n = 9$ cars where blue shading denotes the stable region. Panel (a) shows the slope of the OV function $\mathrm{V}'(h^*)$ as a function of the sensitivity α, where the dashed asymptotes are situated at $\mathrm{V}'(h^*) \simeq 0.5103$, $\mathrm{V}'(h^*) \simeq 0.5431$, $\mathrm{V}'(h^*) \simeq 0.6046$, and $\mathrm{V}'(h^*) \simeq 0.7089$. Panels (b)–(f) show stability diagrams in the (h^*, α)-plane for particular values of v^0 (indicated in each panel), which correspond to $\mathrm{V}'_{\max} \simeq 0.4619$, $\mathrm{V}'_{\max} \simeq 0.5123$, $\mathrm{V}'_{\max} \simeq 0.5627$, $\mathrm{V}'_{\max} \simeq 0.6367$ and $\mathrm{V}'_{\max} \simeq 0.8399$, respectively.

when $\omega \to k\pi/n$; see Fig. 2(a). This means that the curves are ordered from left to right as k increases. When $n \to \infty$, the first asymptote for $k = 1$ converges to $\mathrm{V}'(h^*) \equiv 1/2$, while the last asymptote for $k = n/2$ or $k = (n-1)/2$ converges to $\mathrm{V}'(h^*) \equiv \pi/4$. Further, the $k > 1$ curves accumulate on the $k = 1$ curve when $n \to \infty$. Using the stability criteria presented in [17], one may

show that the stability boundary for the equilibrium is always the first (*i.e.*, $k = 1$) Hopf bifurcation curve. This means that the uniform flow equilibrium (9) is stable to the left of the $k = 1$ Hopf bifurcation curve; see Fig. 2(a). It may also be shown that the uniform flow equilibrium remains unstable to the right of the $k = 1$ curve, and as each of the $k > 1$ curves is crossed from left to right, an extra pair of complex conjugate characteristic exponents crosses into the right-half complex plane.

In Fig. 2 we present stability diagrams for $n = 9$ cars. There are four nested Hopf bifurcation curves corresponding to the four admissible wave numbers $k = 1, 2, 3, 4$. This example is sufficient to give an indication of the structure for large n. The Hopf bifurcation curves are shown in the $(\mathrm{V}'(h^*), \alpha)$-plane in Fig. 2(a). The stability boundary, *i.e.*, the curve for $k = 1$, is the bold curve. The asymptotes are indicated by vertical dashed lines and the blue area is the stable region of the uniform flow equilibrium (9).

Since the first derivative of the OV function (4) has a turning point (see Fig. 1(b)), the $(\mathrm{V}'(h^*), \alpha)$ stability diagram of Fig. 2(a) may be transformed into the (h^*, α)-plane by a sort of 'nonlinear left-to-right folding'. Five qualitatively different configurations are possible and shown in Figs. 2(b)–(f); which situation occurs depends on the value of $\mathrm{V}'_{\max} = (2\sqrt[3]{2}/3)\, v^0$.

The blue area again corresponds to the stability of the uniform flow equilibrium (9) and the curves are nested in strict order from outside to inside as k increases. When $\mathrm{V}'_{\max}$ is to the left of a particular asymptote in the $(\mathrm{V}'(h^*), \alpha)$-plane, the corresponding curve in the (h^*, α)-plane is a single curve with a maximum. On the other hand, when $\mathrm{V}'_{\max}$ is to the right of this asymptote, there are two corresponding curves in the (h^*, α)-plane and each possesses a vertical asymptote. Correspondingly, all curves have maxima in Fig. 2(b) because $\mathrm{V}'_{\max}$ is to the left of the first (bold) Hopf bifurcation curve in Fig. 2(a). When $\mathrm{V}'_{\max}$ exceeds the $\mathrm{V}'(h^*)$ value of the asymptote of a certain stability curve in the $(\mathrm{V}'(h^*), \alpha)$-plane, then the corresponding curve in the (h^*, α)-plane becomes unbounded. Because there are four Hopf bifurcation curves, this analysis leads to the additional four possibilities shown in Fig. 2(c)–(f). The left-hand endpoints of the Hopf bifurcation curves approach $(1, 0)$, while their right-hand endpoints approach $(+\infty, 0)$.

By considering (15) and taking into account the first derivative of the OV function (4), it can be shown that when $\mathrm{V}'_{\max} \geq \pi/4$, that is, $v^0 \geq 3\pi/8\sqrt[3]{2}$, the asymptotes converge to particular values of h^* as $n \to \infty$; see Fig. 2(f) for which $v^0 = 1.0$. Moreover, the $k > 1$ curves accumulate on the $k = 1$ curve when $n \to \infty$.

In the absence of reaction time delay, it may be shown that the Hopf bifurcation curves are straight lines in the $(\mathrm{V}'(h^*), \alpha)$-plane given by $\alpha = 2\cos^2(k\pi/n)\,\mathrm{V}'(h^*)$. As a consequence, the stability diagram in the (h^*, α)-plane is always qualitatively the same as that in Fig. 2(b). Further, for non-zero delay, the Hopf curves are always nested in strict order in the (h^*, α)-plane when $\mathrm{V}'_{\max} \geq \pi/4$ (*i.e.*, $v^0 \geq 3\pi/8\sqrt[3]{2}$). However, when the delay is zero, such a nesting only occurs for sufficiently large v^0. Thus even at the linear level, the inclusion of delay leads to new types of qualitative dynamics.

5 Two-dimensional bifurcation diagrams

The overall goal of this paper is to gain insight into how the qualitative behavior of solutions of the DDE system (1)–(2) depends on the problem parameters, namely the number of cars n, the average headway h^*, the sensitivity α, and the target speed v^0. To simplify matters, we fix $v^0 = 1.0$ in what follows and now consider two-parameter bifurcation diagrams in the (h^*, α)-plane (sometimes called phase-diagrams in the traffic literature). Note that choosing larger values of v^0 does not change the linear stability diagram qualitatively; see Section 4.

Our aim is to show the general trends in the qualitative dynamics as n is increased towards numbers that are more representative of real traffic situations. Since continuation studies with DDE-BIFTOOL are quite intensive in terms of CPU time and memory, the bifurcation analysis for large numbers of cars is unfeasible. We found that the case of $n = 9$ cars is a good compromise — it is sufficiently general to showcase all phenomena in the bifurcation diagram while still being small enough to allow for a full bifurcation analysis. We also considered the maximal case of $n = 17$ cars to check branches of periodic orbits and the scaling of Floquet multipliers.

In Fig. 3 we present three bifurcation diagrams in the (h^*, α)-plane for $n = 3$, $n = 5$ and $n = 9$. We describe the common qualitative features of the two-parameter bifurcation diagrams and then give particular details for each of the cases.

Firstly, the linear theory of Section 4 gives explicit curves in the (h^*, α)-plane where the uniform flow equilibrium loses stability via a Hopf bifurcation that gives rise to oscillations with wave number $k = 1$. These Hopf bifurcation curves are shown in Fig. 3(a)–(c) as bold solid curves and the blue areas indicate where the uniform flow equilibrium is stable. For $n > 3$ cars there is a further set of admissible wave numbers $k = 2, \ldots, (n-1)/2$. (To reduce the number of special cases, we consider only the n odd case.) Linear theory gives explicit curves on which further Hopf bifurcations of the (already unstable)

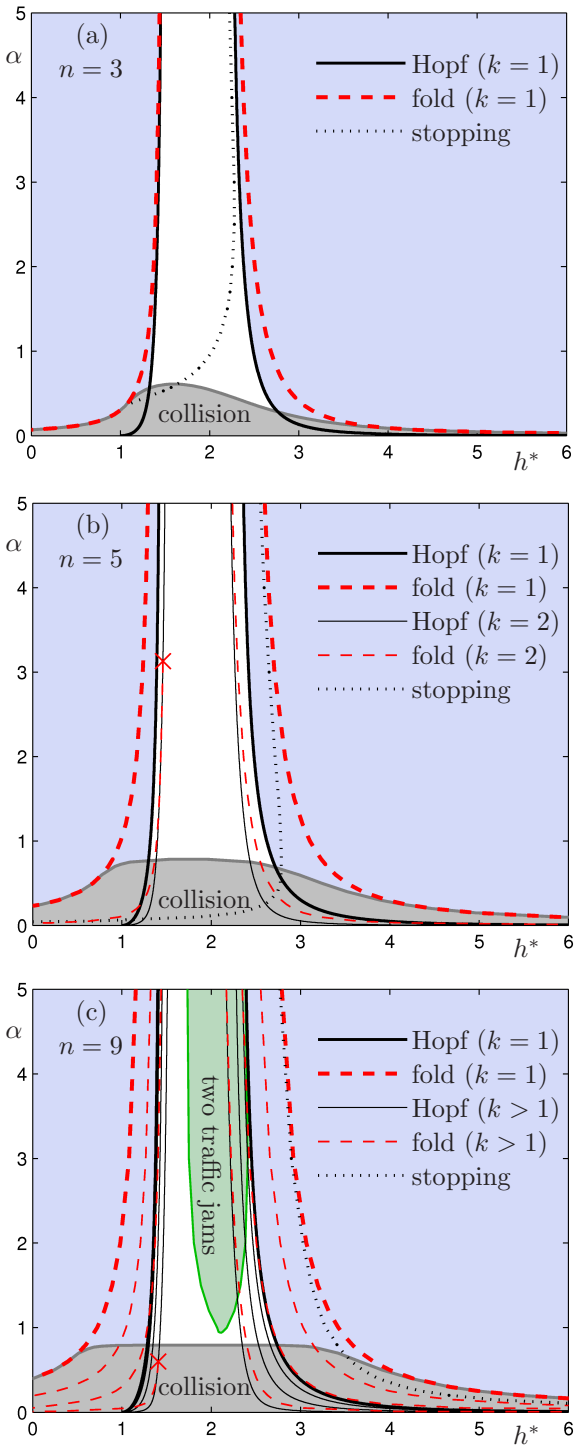

Fig. 3. Two-dimensional bifurcation diagrams in the (h^*, α)-plane for $n = 3$ cars (a), $n = 5$ cars (b), and $n = 9$ cars (c) for target speed $v^0 = 1.0$. At points denoted by red crosses ($\times$) the Hopf bifurcation is degenerate. In panel (c) the region of two traffic jams is defined by the condition $\max|\mu| \leq 1.01$ for the largest Floquet multiplier of periodic solutions for $k = 2$.

uniform flow equilibrium occur (*i.e.*, other complex conjugate pairs of characteristic exponents, corresponding to a mode with wave number k, cross into the right-half plane). These curves are shown in Fig. 3(a)–(c) as thin solid curves.

The Hopf bifurcation curves are nested in strict order so that the $k = 1$ curves are the outermost and the $k = (n-1)/2$ curves are the innermost. Further, for the chosen value $v^0 = 1.0$, the Hopf bifurcation curves all possess vertical asymptotes in the (h^*, α)-plane as in Fig. 2(f), that is, the unstable domains are unbounded in α.

We now use DDE-BIFTOOL to probe the dynamics of the system at the nonlinear level. DDE-BIFTOOL calculates that the Hopf bifurcations are usually subcritical, *i.e.*, the branches of periodic solutions bifurcating from the uniform flow equilibrium are unstable. If one examines the Floquet multipliers of the unstable bifurcating branches in the vicinity of the Hopf bifurcation point, one finds $2k-1$ multipliers outside the unit circle (one real multiplier and $k-1$ complex conjugate pairs); see Section 9.

Furthermore, DDE-BIFTOOL shows that each branch of unstable periodic solutions usually undergoes a fold bifurcation, where the real unstable Floquet multiplier crosses the unit circle inwards at 1. Consequently the $k = 1$ branch becomes stable at this bifurcation, but the $k > 1$ branches remain unstable as they still have $2(k-1)$ Floquet multipliers outside the unit circle.

The fold bifurcation curves are shown in Fig. 3(a)–(c) as red dashed curves and the curves for $k = 1$ are emphasized in bold. The Hopf bifurcation curve for a particular k is nested inside the fold bifurcation curve for the same k, and the fold bifurcation curves themselves are nested in strict order so that the outermost curves belong to $k = 1$ while the innermost curves belong to $k = (n-1)/2$. Further, most of the fold bifurcation curves have vertical asymptotes meaning that the Hopf bifurcation remains subcritical even as $\alpha \to \infty$. However, in some cases the fold bifurcation curves end at a degenerate Hopf bifurcation point, *i.e.*, at a point where a Hopf bifurcation changes from subcritical to supercritical as α is increased: these points are marked by red crosses ($\times$) in Fig. 3(b) and (c). For any given n, degenerate Hopf bifurcation points have only been observed to occur for the largest possible wave number.

Inside the fold curve for $k = 1$, there exists a stable periodic solution. Therefore, in the parameter domain sandwiched between the fold and Hopf bifurcation curves for $k = 1$, the stable periodic solution coexists with the stable uniform flow equilibrium and an unstable periodic solution. In other words, there is bistability in this region. When one carries out an initial value simulation, the precise choice of initial data will select which of the two stable solutions is observed as $t \to \infty$. Furthermore, one encounters hysteresis be-

tween the two solutions when h^* is swept back and forth.

If we enter the parameter domain sandwiched between the fold and Hopf bifurcation curves for $k > 1$, then the only change is in the number of coexisting unstable solutions, and it is not yet clear what this implies for the dynamics. For $k_1 < k_2$, there is no general principle as to whether the Hopf bifurcation curve for k_1 is inside/outside the fold bifurcation curve for k_2, so there is a wide range of possibilities for the combinations of coexisting unstable solutions.

To illustrate the power of our approach we now describe three extra features that we have added in the two-parameter diagrams of Fig. 3.

1. **Collisions**. A feature of the periodic solutions that we have found by continuation is that the headway may pass through zero, which may be interpreted as the case of colliding cars. What is more, the headway may become negative, which is clearly unphysical. To investigate this behavior, we simply extend the definition (4) of the OV function by $V(h) :\equiv 0$ for $h < 0$. The grey curve in Figs. 3(a)–(c) indicates where the the headway first becomes zero on the $k = 1$ stable solution branch. Consequently, we can say that the model is definitely unphysical below the grey curve. The grey curve, which connects the $k = 1$ fold bifurcations curves, appears to converge to a horizontal line as n increases. Consequently, it appears that, in the large n limit, there is a critical α below which the model is unphysical. However, this conclusion is only partial: above the grey line there are most likely solutions with plausible initial data which involve collisions as part of their transient behavior, even though their long-term dynamics is well behaved.

2. **Stopping**. Another interesting feature of the solutions found by continuation is that cars may (almost) come to rest at some point in their period. In fact, model (2) is such that zero velocity cannot be attained in finite time (the decay of the velocity is exponential). We have illustrated this 'near-stopping' behavior in Fig. 3(a)–(c) by adding a dotted curve which, when crossed from right to left results in the minimum velocity of the stable $k = 1$ branch falling below 0.01. When n increases, the dotted curve appears to converge to the right-hand $k = 1$ fold bifurcation curve. Thus it seems that cars always come close to stopping if n is chosen sufficiently large.

3. **Meta-stable pattern formation.** The most important extra feature, which is discussed in detail in Section 9, is the green shading added to part of Fig. 3(c). This shading indicates that the largest Floquet multiplier of the (unstable) $k = 2$ branch has modulus less than 1.01. Consequently, in this region, solutions with initial data chosen sufficiently close to the $k = 2$ unstable periodic solution remain close to that solution for a long time.

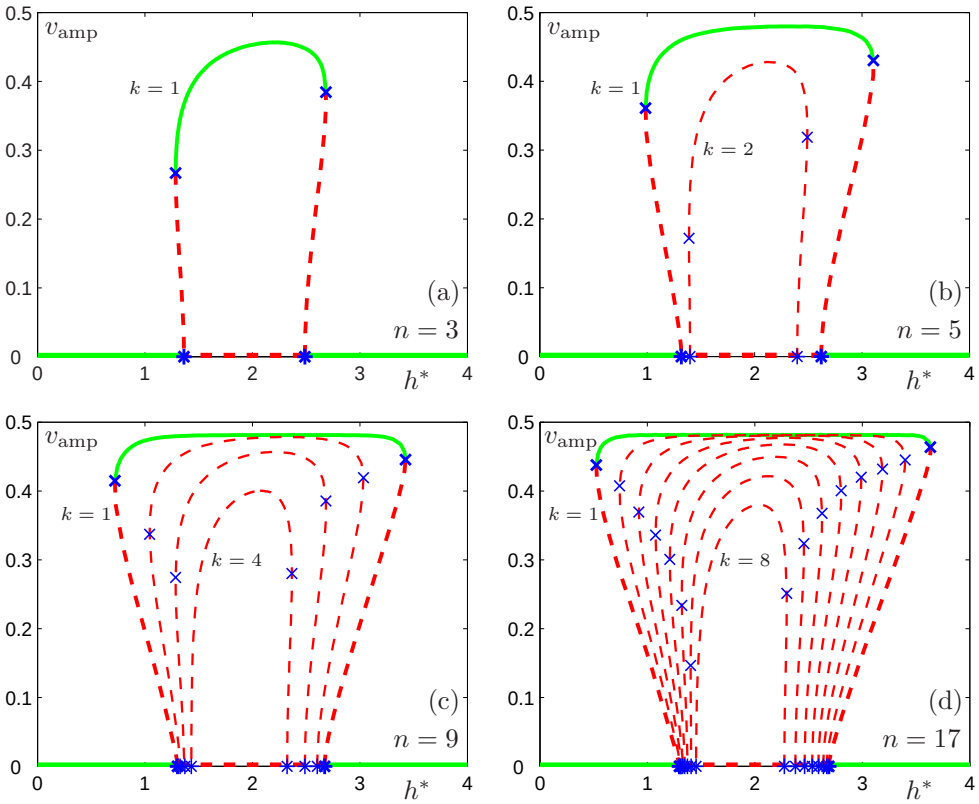

Fig. 4. Branches of solutions as a function of the average headway h^* for $n = 3$ (a), $n = 5$ (b), $n = 9$ (c), and $n = 17$ cars (d); the target speed is $v^0 = 1.0$ and the sensitivity is $\alpha = 1.0$. Stable states are represented by solid green curves, while unstable states by dashed red curves. Hopf bifurcations are depicted as blue stars (*) and fold bifurcations as blue crosses (×).

Therefore, although simulations indicate that the generic $t \to \infty$ behavior is convergence either to the uniform flow equilibrium or the stable $k = 1$ branch, richer possibilities may be observed over intermediately long time scales.

6 Branches of periodic solutions

The bifurcation diagrams in Fig. 3 can be further clarified by fixing α (we take $\alpha = 1.0$) and considering one-parameter bifurcation diagrams where only the parameter h^* is allowed to vary; see Fig. 4. In effect, we consider changes in the dynamics on a one-dimensional horizontal cross-section through Figs. 3(a)–(c). In such pictures the horizontal axis is the average headway h^* and the vertical axis displays a solution norm, which is in our case the amplitude of the velocity oscillations:

$$v_{\text{amp}} = \max_t v(t) - \min_t v(t). \tag{16}$$

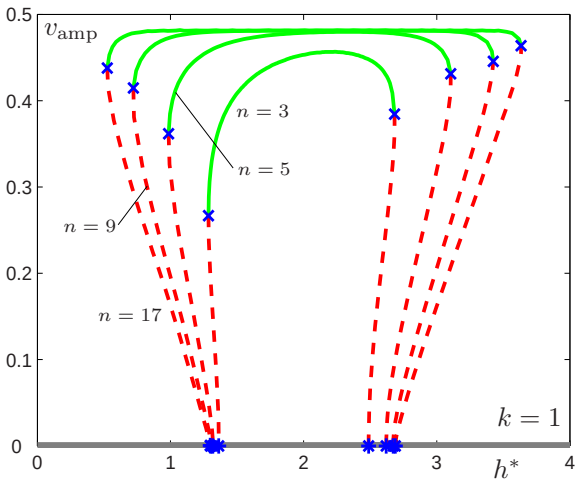

Fig. 5. The $k = 1$ branches from Fig. 4 of periodic solutions for $n = 3$, $n = 5$, $n = 9$ and $n = 17$ cars.

For the uniform flow equilibria we have $v_{\mathrm{amp}} = 0$, while for the periodic solutions that we calculate, the quantity (16) is the same for each car. This is a direct consequence of the $\mathbb{Z}_n$-symmetry

$$v_i(t) = v_{i+1}\left(t - \frac{T}{n}\right), \quad h_i(t) = h_{i+1}\left(t - \frac{T}{n}\right) \tag{17}$$

of the periodic solutions, where T is the period. In other words, it is sufficient to plot the profile of, say, the first car; the profiles for all other cars are simply shifted copies.

The one-parameter continuation results are presented in Fig. 4 for $n = 3$, $n = 5$, $n = 9$ and $n = 17$ cars; panels (a)–(c) correspond to cross sections through Figs. 3(a)–(c). Here green solid curves denote stable solutions whereas red dashed curves denote unstable solutions. Hopf bifurcations of the uniform flow equilibrium are denoted by blue stars (*), and fold bifurcations of the periodic solution are denoted by blue crosses (×). Observe that the uniform flow equilibrium is stable for large and small values of h^* in accordance with Fig. 3. The branches of periodic solutions connect the subcritical Hopf bifurcation points and they are strictly ordered so that the branch for $k = 1$ is the outermost and $k = (n-1)/2$ is the innermost. The only non-trivial stable solutions are those 'at the top' of the $k = 1$ branch, between the fold bifurcation points. An image similar to Fig. 4 for a model without delay can be found in [8]. However, the branches for different k are much more pronounced in our case, which we attribute to the effect of the delay.

Note that there appear to be two types of convergence on the level of the one-parameter bifurcation diagrams. Firstly, Fig. 4 is partial evidence that, as n gets larger and larger, the branch for any fixed $k > 1$ converges, in the pseudonorm defined by (16), to the $k = 1$ branch. Consequently, one might

conclude that for $k = k^* > 1$ and n/k^* sufficiently large, the $k = k^*$ and $k = 1$ branches have significant structural features in common. Secondly, as is illustrated in Fig. 5, it appears that, as n is increased (through $n = 3, 5, 9, 17$), the $k = 1$ branch tends to a limit curve. This limiting behavior might be indicative of travelling wave dynamics since the system, in the large n limit, does not 'feel' (over intermediate time scales) that it is subject to periodic boundary conditions.

7 Periodic solutions with fronts

We now consider how the convergence of the one-parameter bifurcation diagrams manifests itself on the level of the associated oscillations. In Fig. 6 we present the oscillation profile of the $k = 1$ periodic solution for $n = 17$, $n = 9$, $n = 5$ and $n = 3$ cars. The figure is for $h^* = 2.1$; *c.f.* Fig. 5. Plotted are the velocity v_1 and the headway h_1 of the first car, where we chose the maximum of v_1 to be at $t = 0$. In Fig. 6 all panels are drawn on the time scale of the period of the oscillation for $n = 17$. The dashed red lines indicate the period for $n = 9$, $n = 5$ and $n = 3$ in panels (b), (c) and (d), respectively. The profile for $k = 1$ corresponds to a situation where the cars have (practically) zero velocity for part of the period of the oscillation. The figure indicates that there is a convergence of the profiles with n: the oscillation develops fronts that connect the region with (practically) zero velocity to a plateau with an (almost) constant maximal velocity. Similarly, the headway develops two regions with almost constant (small or large) headways. We distinguish *stop-fronts* connecting high velocity to almost zero velocity, and *go-fronts* connecting almost zero velocity to high velocity. Both types of fronts appear to tend to a limit shape as n is increased; this is why we plotted all profiles in Fig. 6 on the same time-scale.

In Fig. 7 we consider how the oscillations for fixed $h^* = 2.1$ and $n = 17$ depend on the wave number k. The representation is as in Fig. 6, meaning that all panels are drawn on the time scale of the period of the $k = 1$ oscillation. As k decreases one notices again that the fronts between different plateaux appear to converge in profile: the main difference between the cases is the length of the plateaux. The period of oscillations satisfies

$$T \simeq C \frac{n}{k} \tag{18}$$

for a constant $C = C(h^*, \alpha, v^0)$ that depends on all parameters; this was checked numerically with the available data.

While the continuation approach taken here limits n to relatively small values, Figs. 6 and 7 still clearly suggest a convergence of the $k = 1$ solution to some

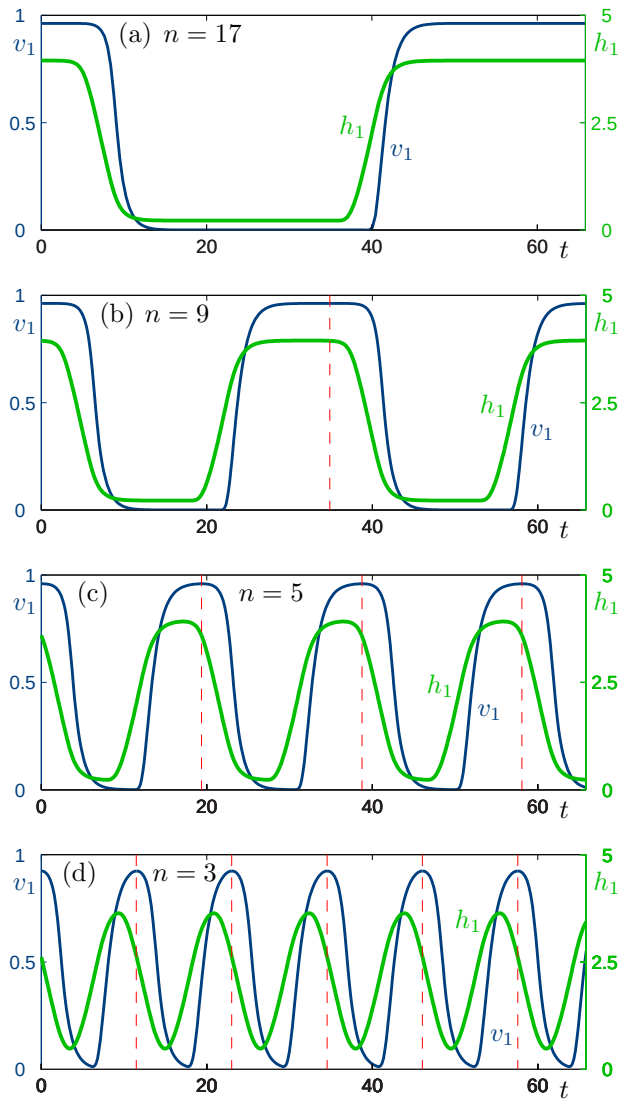

Fig. 6. Oscillation profiles for wave number $k = 1$ and for $n = 17$ (a), $n = 9$ (b), $n = 5$ (c), and $n = 3$ (d) cars; the target speed is $v^0 = 1.0$, the sensitivity is $\alpha = 1.0$, and the average headway is $h^* = 2.1$. The velocity v_1 of the first car is shown in dark blue to the scale on the left; the headway h_1 of the first vehicle is shown in green to the scale on the right. All panels are shown on the scale of one period of $T \simeq 65.8171$ for $n = 17$; the other periods of $T \simeq 34.8447$ for $n = 9$, $T \simeq 19.3540$ for $n = 5$, and $T \simeq 11.5445$ for $n = 3$ are indicated by red dashed vertical lines. Notice the convergence of the stop- and go-fronts, that is, the parts of the orbits that connects the plateaux.

limiting shape as $n \to \infty$, as well as a convergence of the oscillations for other wave numbers to that for $k = 1$ as $n/k \to \infty$. As we will see in the next section, this has important consequences in terms of transient traffic jams. Note that identifying the mathematical limit and, in particular, the exact scaling of the fronts, remains an interesting challenge beyond the bifurcation study presented here.

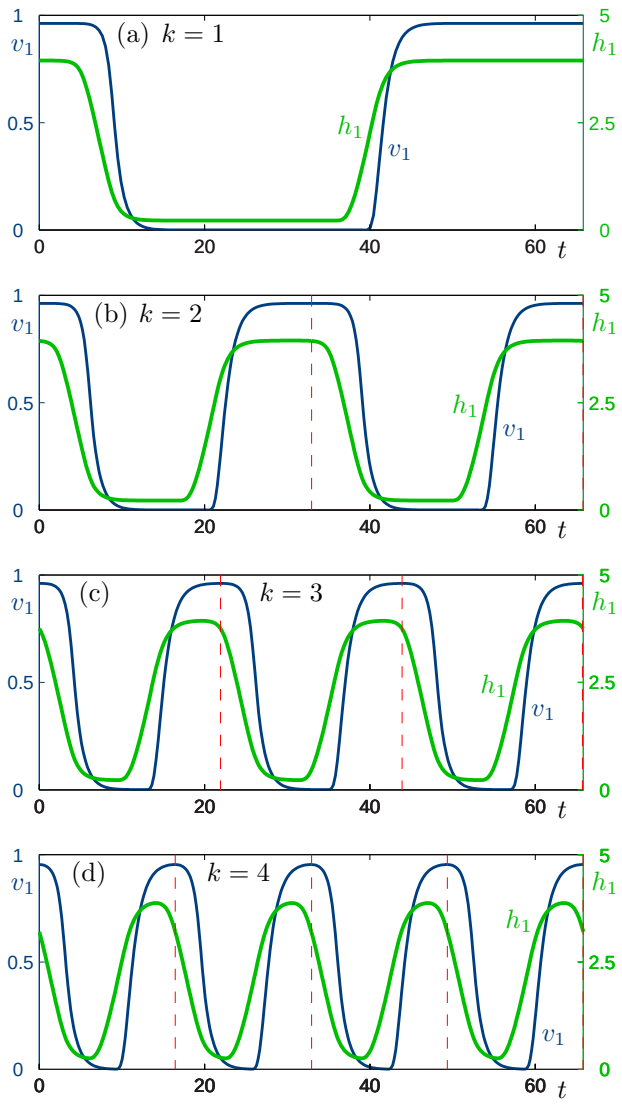

Fig. 7. Oscillation profiles for $n = 17$ and for wave numbers $k = 1$ (a), $k = 2$ (b), $k = 3$ (c), and $k = 4$ (d); the target speed is $v^0 = 1.0$, the sensitivity is $\alpha = 1.0$, and the average headway is $h^* = 2.1$. The velocity v_1 of the first car is shown in dark blue to the scale on the left; the headway h_1 of the first vehicle is shown in green to the scale on the right. All panels are shown on the scale of one period of $T \simeq 65.8171$ for $k = 1$; the other periods of $T \simeq 32.908$ for $k = 2$, $T \simeq 21.9379$ for $k = 3$, and $T \simeq 16.4403$ for $k = 4$ are indicated by red dashed vertical lines. Notice the convergence of the stop- and go-fronts, that is, the parts of the orbits that connects the plateaux.

8 Floquet multipliers and eigendirections

We now look more closely at the stability properties of the different periodic solutions. In Fig. 8 the modulus $|\mu|$ of the corresponding leading Floquet multipliers are depicted as a function of the headway h^* for the representative

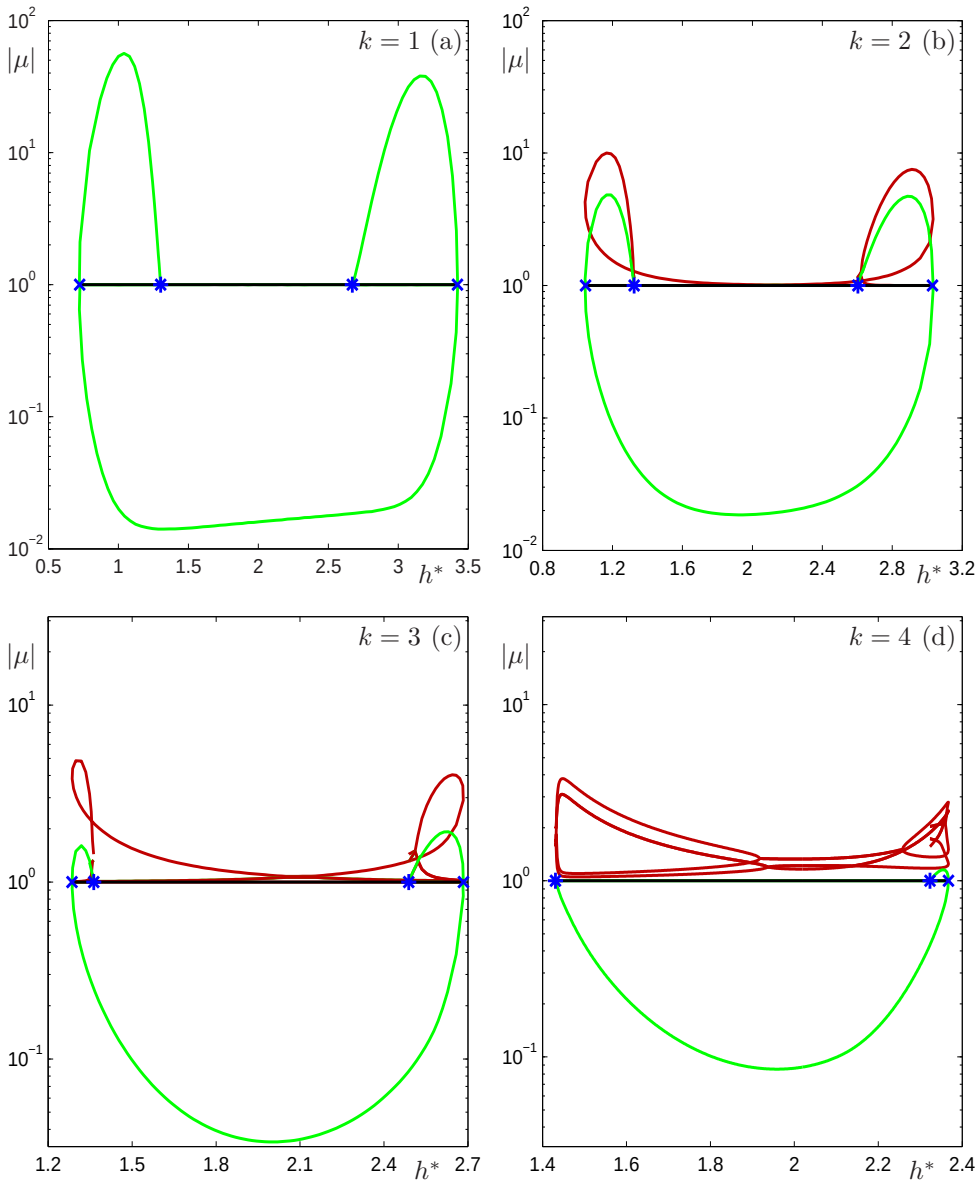

Fig. 8. Modulus $|\mu|$ of the leading Floquet multiplier as a functions the average headway h^* in case of $n = 9$ cars for wave numbers $k = 1$ (a), $k = 2$ (b), $k = 3$ (c), and $k = 4$ (d). This corresponds to the branches of periodic solutions shown in Fig. 4(c); we have $v^0 = 1.0$ and $\alpha = 1.0$. Hopf and fold bifurcation points are denoted by blue stars (*) and blue crosses (×), respectively.

case of $n = 9$ cars for the wave numbers $k = 1, 2, 3, 4$. Recall from Section 3 that the infinitely many Floquet multipliers have the origin in the complex plane as their only accumulation point; all Floquet multipliers that are not shown in Fig. 8 have modulus less than one for all values of h^*. The leading Floquet multipliers in panels (a)–(d) were computed with DDE-BIFTOOL as part of the stability analysis along the branches shown in Fig. 4(c). To bring out the features, we use a logarithmic scale along the vertical axis. For any k, at the Hopf bifurcation points there are two Floquet multipliers at 1 and

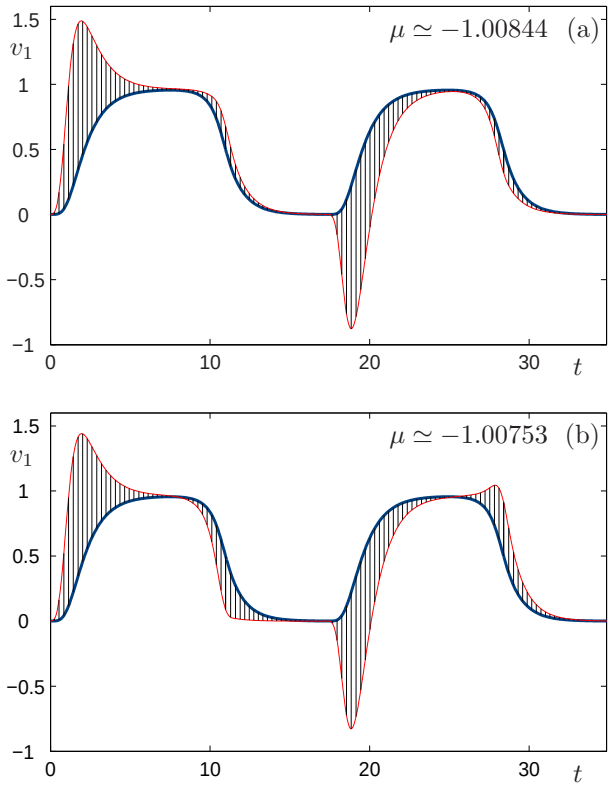

Fig. 9. Eigendirection in the form of a direction field plotted over twice the period of the periodic solutions with the Floquet multipliers $\mu \simeq -1.00844$ (a) and $\mu \simeq -1.00753$ (b). The panels show the projection onto the velocity v_1 of the first car for $n = 9$, $k = 2$, $v^0 = 1.0$, $\alpha = 1.0$, and $h^* = 2.1$.

another $(k-1)$ complex conjugate pairs of Floquet multipliers outside the unit circle. One multiplier (green curve) moves outside the unit circle at the subcritical Hopf bifurcations and then crosses into the unit circle at the fold bifurcations. Similarly, the other leading multipliers for $k > 1$ appear outside the unit circle at their subcritical Hopf bifurcations, but then stay outside the unit circle over the entire range of h^*. In other words, Fig. 8 gives a different representation of the fact that all periodic orbits are unstable for $k > 1$. For even k we observe that one of the complex pairs of these Floquet multipliers may come together and produce two real Floquet multipliers. For n/k large enough this happens close to the Hopf bifurcation point.

However, Fig. 8(b) also shows that the oscillation for $k = 2$ is almost stable around the point $h^* = 2.1$; at this point the two unstable eigenvalues are actually real and negative, namely $\mu \simeq -1.00844$ and $\mu \simeq -1.00753$. By setting a threshold for $\max|\mu|$ one can quantify the 'almost-stability' of the periodic orbit for $k = 2$: inside the green shaded region in Fig. 3(c) we have that $\max|\mu| \leq 1.01$. While this bound is somewhat arbitrary, we found by numerical simulation that traffic jams corresponding to $k = 2$ periodic orbits exist in this parameter region for long periods of time; see Section 9 for more

details on the connection between periodic solutions and traffic jams. More generally, there is a region around $h^* = 2.1$ where the unstable waves for any k are 'least unstable'. Our numerical results indicate that this effect is more pronounced the larger the number of cars n.

The instability of a weakly periodic orbit is very small, but it is not 'spread evenly' around the periodic orbit. To show this we present in Fig. 9 the eigendirection associated with the two unstable Floquet multipliers $\mu \simeq -1.00844$ and $\mu \simeq -1.00753$ of the weakly unstable periodic orbit for $n = 9$ and $k = 2$. It is computed and represented by DDE-BIFTOOL in the form of a direction field that shows how a vector changes along the periodic orbit under the action of the variational equation [11]. We show the unstable direction with respect to the velocity profile of the first car. The Floquet multiplier measures the expansion (which is practically nonexistent in our case of Floquet multipliers that are almost 1 in magnitude) of a vector as the flow is followed along the periodic orbit. The data in Fig. 9 is plotted over two periods, because the most unstable Floquet multipliers are negative: the vectors forming the eigendirections close up after two periods. In Fig. 9 only the vectors at the mesh points are shown and the red curve is the envelope of all vectors.

Both periodic orbits are most unstable near the fronts between the plateaux. This indicates that any eventual instability is due to the motion of the fronts. Notice the difference between the two cases in Fig. 9(a) and (b) in terms of the direction of motion of the stop-fronts. As we will see in the next section, front dynamics is responsible for merging or dispersing traffic jams.

We now show that we can extract from the bifurcation analysis the asymptotics of the modulus $|\mu^{(n,k)}|$ of the largest Floquet multiplier, as a function of n and k. Different waves interact via an overlap of their exponentially decaying tails. Consequently, we make the ansatz that there is an exponential relationship of the form

$$\max |\mu^{(n,k)}| - 1 = R\, e^{-q\frac{n}{k}}\,, \tag{19}$$

when n is large and k is small enough; *c.f.* [12,13]. Clearly, the constants q and R generally depend on the parameters v^0, α, h^*.

We test this ansatz in Fig. 10 where we plot $\max |\mu^{(n,k)}| - 1$ on a logarithmic scale as a function of n/k, where n varies for $k = 2$ in panel (a) and k varies for $n = 17$ in panel (b). The blue line is the least-square fitting through all but the first data point, which we disregarded as exceptional in terms of the convergence effect for $n/k \to \infty$ that we are interested in. The resulting values of q and $\ln R$ for both cases are shown in Table 1. Together with the good fit of the blue lines in Fig. 10, this is numerical evidence that the largest Floquet multiplier scales (for fixed parameters) as given by Eq. (19). Note that the data presented in Fig. 10 constitutes the state of the art of what can be achieved with the standard DDE-BIFTOOL implementation on a single workstation.

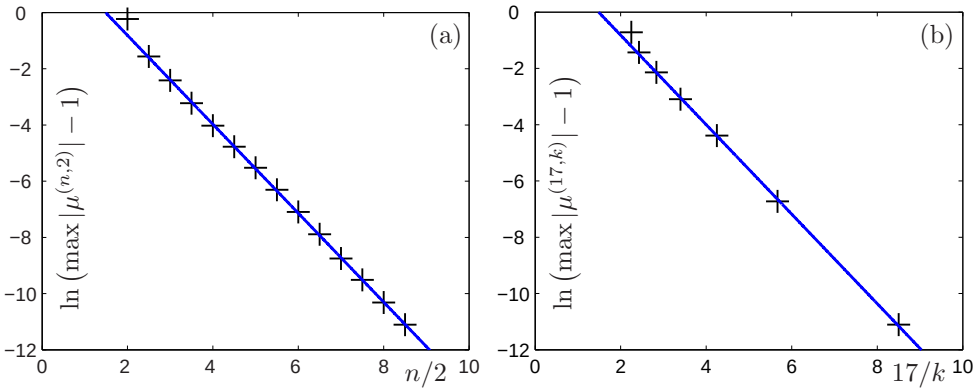

Fig. 10. The logarithm of the deviation of the modulus of the largest Floquet multiplier from 1 as a function of n/k for the periodic solutions for $v^0 = 1.0$, $\alpha = 1.0$, and $h^* = 2.1$. Panel (a) shows a plot for fixed $k = 2$ and varying n, and panel (b) for fixed $n = 17$ and varying k. The blue curve is a least square fit (omitting the first data point); see also Table 1.

Table 1
Least-square fitted constants appearing in (19) for the periodic solutions for $v^0 = 1.0$, $\alpha = 1.0$, and $h^* = 2.1$.

	$k = 2 \quad (n = 5, \ldots, 17)$	$n = 17 \quad (k = 2, \ldots, 7)$
q	-1.5816 ± 0.0053	-1.5901 ± 0.0121
$\ln R$	2.3522 ± 0.0308	2.3616 ± 0.0601

9 Traffic jams as long transients

In our model, a traffic jam is a region of the ring along which the cars are almost stationary (velocity of less than 0.01 according to our definition). Hence, the location of traffic jams can best be seen in a plot of the positions x_i of all cars. As cars enter a traffic jam at the back and leave it at the front, traffic jams move with a certain speed against the direction of traffic along the ring. An overall traffic pattern consists of a finite number of traffic jams that all move with their own different (but typically similar) speeds. A traffic jam can dissolve or merge with another traffic jam of a different speed when they meet. Hence, there is an evolution of the traffic pattern until a stable pattern has been reached.

Of importance is the relationship between a traffic pattern and the trajectory of an individual car. A stable traffic pattern corresponds to a stable periodic orbit for the motion of the cars. Hence, the only stable traffic pattern in our model is that corresponding to stable $k = 1$ oscillations. Because the fronts of traffic jams move only very slowly along the ring, the time it takes the car to drive around the circuit is close but slightly different from the period of the periodic oscillations of its velocity and headway. Similarly, if the pattern

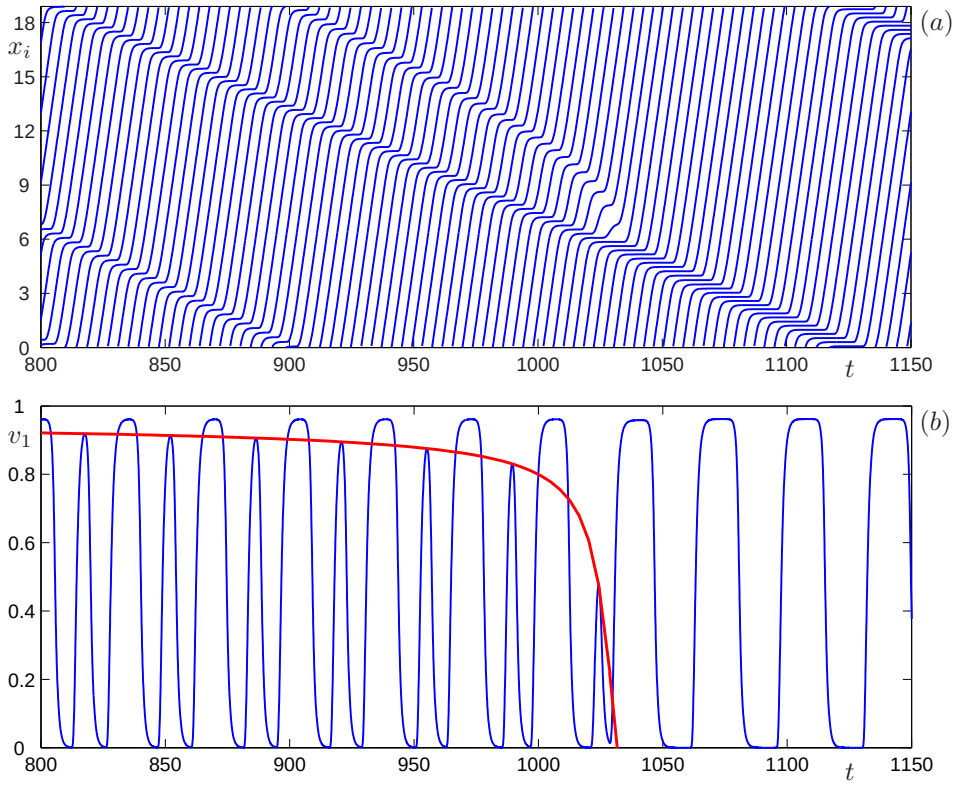

Fig. 11. Plot of the positions x_i of all $n = 9$ cars (a), and velocity v_1 of the first car (b), when two traffic jams merge; the other parameters are $v^0 = 1.0$, $\alpha = 1.0$, $h^* = 2.1$.

is not stable, a car almost has the same velocity and headway profile from round to round. In particular, unstable periodic orbits are related to unstable traffic patterns. As we will see now, weakly unstable periodic orbits give rise to traffic jams that can persist as long transients. The motion of the traffic jams is closely related to the motion of the fronts of the almost periodic dynamics of the cars.

When one starts an initial value simulation of the system from suitably random initial data, unstable waves form and will eventually die out. (Specifically, we start from equidistant cars with velocities chosen randomly and uniformly from $[0, v^0]$, and integrate the system with an explicit Euler method with time step 0.02.) As was mentioned in Section 8, already for $n = 9$ cars we find that waves for $k = 2$, corresponding to two traffic jams along the ring, may survive for considerable amounts of time. In other words, weakly unstable traffic jams appear as long transients. When they eventually disappear this can happen in only two competing ways, which are shown in Figs. 11 and 12, respectively.

In the case shown in Fig. 11 a traffic jam catches up with another traffic jam and the two then merge; see the plot of the positions in panel (a). At the same time, panel (b) shows the velocity profile of the first car. Fig. 11 shows that the

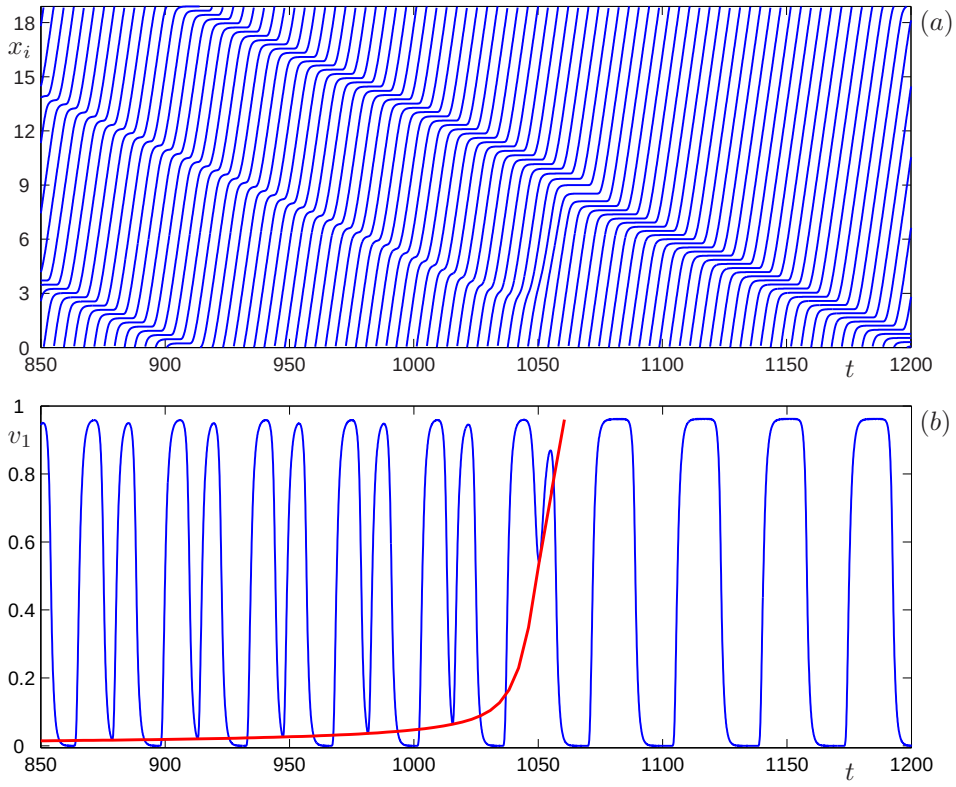

Fig. 12. Plot of the positions x_i of all $n = 9$ cars (a), and the velocity v_1 of the first car (b), when a traffic jam disperses; the other parameters are $v^0 = 1.0$, $\alpha = 1.0$, $h^* = 2.1$.

go-front of the first and the stop-front of the second traffic jam 'move towards one another' and then disappear. As a consequence, the region between the two traffic jams of flowing traffic (large velocity) disappears. This behavior is indicative of an unstable eigendirection of the periodic orbit for $k = 2$ as shown in Fig. 9(a), where the stop-front and the go-front move in the same direction (along the periodic orbit). As the two traffic jams move closer together the maximum speed between them decreases. The envelope of these maxima (red curve) diverges more and more from the maximum velocity elsewhere along the ring. Thus, the time until complete merging can be defined as the moment that this envelope reaches zero velocity. The envelope actually describes the local maximum of the velocity for all cars; note that the velocities profiles of the other cars are very similar, but are not shifted copies, since the dynamics is not perfectly periodic.

In contrast, Fig. 12 shows a situation where the traffic jam 'survives' long enough, meaning that it does not merge with another traffic jam, and then disperses. This has only a slight influence of the 'neighboring' traffic jam, as can be seen from the positions in panel (a). As is shown in panel (b), the minimum velocity of cars in this dispersing traffic jam increases, which is again indicated by the envelope (red curve). In this case, the stop-front and

the go-front of one and the same traffic jam slowly 'move closer together', so that the traffic jam eventually disappears. This is associated with an unstable eigendirection of the $k = 2$ periodic orbit as in Fig. 9(b), where the stop-front and the go-front move in opposite directions (along the periodic orbit). The envelope of minima, which also describes the minima for all cars, diverges from being practically zero and complete dispersion is reached when it reaches the maximum velocity on the ring.

10 Conclusion and Discussion

In this paper we considered a car-following model for n cars on a single-lane ring road where the reaction time delay of drivers is included. A bifurcation analysis for increasing numbers of cars brought out convergence effects in two-dimensional and one-dimensional bifurcation diagrams, as well as of oscillation profiles corresponding to traffic jams. We also showed that unstable oscillations for higher wave numbers are only very weakly unstable in a certain parameter region, so that the associated traffic jams can be observed as very long transients. Such traffic jams finally disappear by dispersing or by merging with another traffic jam.

We believe that our study shows the value of continuation methods for the study of traffic models, in particular, in the presence of a delay. The computation of periodic orbits and their stability is an important tool for understanding the evolution of traffic patterns. Indeed, similar low-dimensional slow dynamics seems to appear in many other car-following models as well. Therefore, the continuation techniques used here may help to discover the underlying low-dimensional dynamics in other cases as well.

A limitation is that continuation for DDEs is very demanding in terms of memory and computation time. The computations of branches of periodic orbits and their Floquet multiplier for 17 cars (that is, for a 33 equation DDE system) are at the limit of what can be achieved with the present implementation of DDE-BIFTOOL on a workstation. It would be very interesting to investigate further the observed convergence phenomena for much larger values of n, say, for a few hundred cars . This would be an interesting test case application for algorithms for the numerical stability analysis of a large-scale delay systems that are presently being developed [20,21].

A challenging subject for future research is the analysis of the convergence phenomena that we found. In particular, it appears to be feasible to derive a mathematical model for the front dynamics of traffic jams in the large n limit. The issue here is that the cars 'feel' less and less that they are on a ring. In other words, in the large n limit over intermediately long time scales the

periodic boundary condition will not play a role.

Acknowledgments

The authors thank Jan Sieber, Róbert Szalai, and Róbert Vértesi for helpful discussions. The research of G. O. was supported by ORS Award 2002007025 and a UoB Postgraduate Research Scholarship. The research of B. K. was supported by an EPSRC Advanced Research Fellowship.

References

[1] L. C. Davis, Modification of the optimal velocity traffic model to include delay due to driver reaction time, Physica A 319 (2003) 557–567.

[2] M. Bando, K. Hasebe, K. Nakanishi, A. Nakayama, Analysis of optimal velocity model with explicit delay, Physical Review E 58 (5) (1998) 5429–5435.

[3] M. Bando, K. Hasebe, A. Nakayama, A. Shibata, Y. Sugiyama, Dynamical model of traffic congestion and numerical simulation, Physical Review E 51 (2) (1995) 1035–1042.

[4] K. Nagel, M. Schreckenberg, A cellular automaton model for freeway traffic, Journal de Physique I 12 (2) (1992) 2221–2229.

[5] B. S. Kerner, P. Konhäuser, Cluster effect in initially homogeneous traffic flow, Physical Review E 48 (4) (1993) R2335–R2338.

[6] D. Helbing, Traffic and related self-driven many-particle systems, Reviews of Modern Physics 73 (4) (2001) 1067–1141.

[7] G. Orosz, R. E. Wilson, B. Krauskopf, Global bifurcation investigation of an optimal velocity traffic model with driver reaction time, Physical Review E 70 (2) (2004) 026207.

[8] I. Gasser, G. Sirito, B. Werner, Bifurcation analysis of a class of 'car-following' traffic models, Physica D 197 (3-4) (2004) 222–241.

[9] K. Engelborghs, T. Luzyanina, D. Roose, Numerical bifurcation analysis of delay differential equations using DDE-BIFTOOL, ACM Transactions on Mathematical Software 28 (1) (2002) 1–21.

[10] K. Engelborghs, T. Luzyanina, G. Samaey, DDE-BIFTOOL v. 2.00: a Matlab package for bifurcation analysis of delay differential equations, Tech. Rep. TW-330, Department of Computer Science, Katholieke Universiteit Leuven, Belgium, `http://www.cs.kuleuven.ac.be/~koen/delay/ddebiftool.shtml` (2001).

[11] K. Green, B. Krauskopf, K. Engelborghs, One-dimensional unstable eigenfunction and manifold computations in delay differential equations, Journal of Computational Physics 197 (1) (2004) 86–98.

[12] J. Carr, R. L. Pego, Metastable patterns in solutions of $u_t = \varepsilon^2 u_{xx} - f(u)$, Communications on Pure and Applied Mathematics 42 (5) (1989) 523–576.

[13] J. Carr, R. L. Pego, Invariant manifolds for metastable patterns in $u_t = \varepsilon^2 u_{xx} - f(u)$, Proceedings of the Royal Society of Edinburgh, A: Mathematics 116 (1-2) (1990) 133–160.

[14] O. Diekmann, S. A. van Gils, S. M. Verduyn Lunel, H. O. Walther, Delay Equations: Functional-, Complex-, and Nonlinear Analysis, Vol. 110 of Applied Mathematical Sciences, Springer-Verlag, New York, 1995.

[15] J. K. Hale, L. T. Magelhães, W. M. Oliva, Dynamics in Infinite Dimensions, 2nd Edition, Vol. 47 of Applied Mathematical Sciences, Springer-Verlag, New York, 2002.

[16] J. K. Hale, S. M. Verduyn Lunel, Introduction to Functional Differential Equations, Vol. 99 of Applied Mathematical Sciences, Springer-Verlag, New York, 1993.

[17] G. Stépán, Retarded Dynamical Systems: Stability and Characteristic Functions, Vol. 210 of Pitman Research Notes in Mathematics, Longman, Essex, England, 1989.

[18] T. Insperger, G. Stépán, Updated semi-discretization method for periodic delay-differential equations with discrete delay, International Journal for Numerical Methods in Engineering 61 (1) (2004) 117–141.

[19] E. J. Doedel, A. R. Champneys, T. F. Fairgrieve, Y. A. Kuznetsov, B. Sandstede, X. Wang, AUTO97: continuation and bifurcation software for ordinary differential equations, Tech. rep., Department of Computer Science, Concordia University, `http://indy.cs.concordia.ca/auto/` (1997).

[20] K. Verheyden, K. Green, D. Roose, Numerical stability analysis of a large-scale delay system modeling a lateral semiconductor laser subject to optical feedback, Physical Review E 69 (3) (2004) 036702.

[21] K. Verheyden, K. Lust, A Newton-Picard collocation method for periodic solutions of delay differential equations, Tech. Rep. TW-357, Department of Computer Science, Katholieke Universiteit Leuven, Belgium, `http://www.cs.kuleuven.ac.be/publicaties/rapporten/tw/TW357.abs.html` (2004).